Environment International 209 (2026) 110186

Contents lists available at ScienceDirect

Environment International

journal homepage: www.elsevier.com/locate/envint

Full length article

Black carbon is detectable in association with small extracellular vesicles in fetal circulation

Houman Kahroba [a,b,**], Kenneth Vanbrabant [a], Julian Krauskopf [b], Jacco Briedé [b], Marcel Ameloot [c], Michelle Plusquin [a], Maarten Roeffaers [d], Theo M. de Kok [b], Tim Nawrot [a,e,*]

[a] Centre for Environmental Sciences, Hasselt University, Hasselt, Belgium
[b] Department of Translational Genomics, GROW School of Oncology and Reproduction, Maastricht University, Maastricht, the Netherlands
[c] Biomedical Research Institute, Hasselt University, Agoralaan Building C, 3590 Diepenbeek, Belgium
[d] Department of Microbial and Molecular Systems, KU Leuven, Leuven, Belgium
[e] School of Public Health, Occupational & Environmental Medicine, Leuven University, Leuven, Belgium

ARTICLE INFO

Keywords:
Black carbon
Small extracellular vesicles
Exosomes
Trans-placental transport
Neurodevelopment
Environmental nanoparticles

ABSTRACT

Prenatal exposure to ambient air pollution, particularly black carbon (BC), has been linked to adverse pregnancy outcomes and life-long neurodevelopmental disorders. Yet the mechanism by which inhaled nanoparticles cross the placenta and reach fetal tissues is unclear. Here we show that black carbon (BC) is detectable in association with small extracellular vesicles (sEVs) in fetal circulation and in tissue-enriched sEV subsets. Using label-free two-photon microscopy, we visualised BC associated with individual sEVs isolated from cord-blood plasma of 20 mother-infant pairs. BC-sEV association occurred in 27 % of total cord-blood sEVs, 54 % of placental alkaline-phosphatase-positive ($PLAP^+$) placental vesicles and 68 % of fetal-brain-derived ($Contactin\text{-}2^+$) vesicles. Among BC-positive fetal-brain sEVs, >90 % of the vesicle fluorescence co-localised with BC, demonstrating extensive pollutant loading. These findings provide evidence that BC can be detected in association with sEV-enriched preparations in fetal circulation, consistent with a possible role for sEV-associated carriage following trans-placental particle transfer, though the dominant transport mechanism remains unestablished.

1. Introduction

Globally, approximately 53 million children experience neuro-developmental delays (Olusanya et al., 2018), raising concerns about their cognitive, behavioral, and overall quality of life. (Deng et al., 2025) Among the various environmental factors implicated in neuro-developmental impairment, ambient air pollution has emerged as a critical concern, with evidence suggesting that it may disrupt brain development through mechanisms involving neuroinflammation, oxidative stress, and microglial activation. (Yi et al., 2022) Epidemiological studies have further indicated that prenatal exposure to fine particulate matter is inversely associated with neurodevelopmental outcomes in children. (Hurtado-Díaz et al., 2021; Xu et al., 2022; Lei et al., 2022) However, given that the fetal brain undergoes rapid and dynamic maturation well into early childhood (Binter et al., 2022), the fetal brain remains within a critical window of neurodevelopment beyond the prenatal stage. Furthermore, the neurodevelopmental impact of air pollution exposure may vary depending on the specific timing and duration of exposure across distinct developmental periods, encompassing both prenatal and early postnatal stages. (Deng et al., 2025).

Among these pollutants, black carbon (BC), a major component of fine particulate matter ($PM_{2.5}$) produced by incomplete combustion of fossil fuels and biomass, is of particular concern due to its small size and ability to penetrate biological barriers including placental and blood brain barriers. (Cheng et al., 2023; Vanbrabant et al., 2024) Particulate matter is categorized by size: PM_{10} (particles $\leq$ 10 μm), $PM_{2.5}$ (particles $\leq$ 2.5 μm), and ultrafine particles $PM_{0.1}$ (particles $\leq$ 0.1 μm). (Benabed and Boulbair, 2022) Prenatal exposure to air pollution has been linked to adverse pregnancy outcomes and developmental issues in fetuses,

* Corresponding author at: Centre for Environmental Sciences, Hasselt University, Agoralaan Building D, 3590 Diepenbeek, Belgium.
** Corresponding author at: Department of Translational Genomics, Maastricht University, Centre for Environmental Sciences, Hasselt University, Agoralaan Building D, 3590 Diepenbeek, Belgium.
E-mail addresses: h.kahroba@maastrichtuniversity.nl, houman.kahroba@uhasselt.be (H. Kahroba), tim.nawrot@uhasselt.be (T. Nawrot).

https://doi.org/10.1016/j.envint.2026.110186
Received 4 July 2025; Received in revised form 19 February 2026; Accepted 4 March 2026
Available online 7 March 2026

including low birth weight, preterm birth, and neurodevelopmental disorders. (Nyadanu et al., 2022) The fetal period represents a critical window of vulnerability to environmental exposures, with long-term health consequences originating from in utero conditions. (Martin-Bassols et al., 2023) Higher prenatal exposure to air pollutants, especially in mid-to-late pregnancy, has been linked to lower motor, cognitive, and language scores at age 2 (Loftus et al., 2019), and increased attention deficit hyperactivity disorder-like behaviors by age 3. (Liu et al., 2022) Studies mainly focus on school-aged children (6–12 years), showing associations between prenatal polycyclic aromatic hydrocarbons (PAH) exposure and reduced white matter at age 8 (Peterson et al., 2015; Guxens et al., 2018; Peterson et al., 2022), $PM_{2.5}$ with cortical thinning and altered brain organization at 6–14 years (Peterson et al., 2015; Guxens et al., 2018; Peterson et al., 2022), and PM_{10} with lower IQ at 4–6 years. (Loftus et al., 2019; Porta, 2016) In younger children, prenatal NO_2 exposure correlates with poorer cognition at ~ 14 months (Guxens et al., 2012) and global psychomotor delays at 1–6 years (Guxens et al., 2014), while PAH exposure is linked to cognitive deficits at age 3. (Perera et al., 2006) These findings suggest air pollution exposure during critical periods can disrupt neurodevelopment with lasting effects.

While the placenta serves as a crucial interface regulating nutrient and waste exchange during pregnancy, recent studies from our team have demonstrated that BC particles not only traverse the placental barrier but are also detectable on the fetal side of the placenta. (Bové et al., 2019) Moreover, BC particles have been identified in umbilical cord-blood, as well as in critical fetal organs such as the liver, lungs, and brain, underscoring the far-reaching implications of prenatal exposure. (Bongaerts et al., 2022) Proposed mechanisms for this translocation include endocytosis, transcytosis (Buerki-Thurnherr et al., 2012), interaction with placental macrophages (Liu et al., 2021), and inflammation-induced increases in placental permeability (Pietroiusti et al., 2018).

Small extracellular vesicles (sEVs), also known as exosomes, are nanoscale (~100 nm) lipid bilayer-enclosed vesicles released by cells. Their capacity to traverse biological barriers and mediate intercellular transport has positioned sEVs as potential carriers for various substances, including DNA, RNA, miRNA and proteins. (Di Bella, 2022) Placenta-derived sEVs play critical roles in maternal-fetal communication and can reflect placental function, with biomarkers like placental alkaline phosphatase (PLAP) serving as specific identifiers of placental sEVs. (Burkova et al., 2021) Similarly, neuronal cell adhesion molecules such as Contactin-2 (TAG1) facilitate the identification of fetal-brain-derived sEVs. (Goetzl et al., 2021).

Building upon evidence that ambient BC particles have been detected in human placentae, with placental BC load positively correlating with maternal exposure levels (Bongaerts et al., 2022), and that maternal microbiota-derived sEVs have been identified in amniotic fluid, suggesting their capability to access the fetal environment (Kaisanlahti et al., 2023), this pilot study within the ENVIRONAGE birth cohort aims to elucidate the role of sEVs in mediating the translocation of BC particles from maternal circulation to the fetus. We will analyze 30 samples from 20 mother-infant pairs, encompassing cord-blood total sEVs, placental sEVs, and fetal-brain-derived sEVs. Employing advanced two-photon microscopy techniques, we aim to ascertain whether sEVs act as vectors for BC particles, thereby enabling their passage across the maternal-fetal interface and potentially augmenting fetal exposure to these pollutants. This research endeavors to deepen our comprehension of the mechanisms underlying fetal exposure to airborne pollutants and to inform strategies aimed at mitigating associated health risks.

2. Methods

2.1. Study design and participants

This study was conducted as part of the ENVIRONAGE birth cohort, an ongoing prospective cohort initiated in 2010 at East-Limburg Hospital (Genk, Belgium) to investigate the impact of early-life environmental exposures on health outcomes. Ethical approval for the study was obtained from the Hasselt University and East-Limburg Hospital Ethics Committees (EudraCT B37120107805), and all participants provided informed consent, in accordance with the Declaration of Helsinki (Janssen et al., 2017).

2.2. Sample selection and biobanking (ENVIRONAGE)

For the present analysis, we selected a subset of mother-infant pairs from the ENVIRONAGE birth cohort (initiated in February 2010) based on study-specific criteria, including a range of prenatal BC exposure levels (see below). In total, 20 cord-blood samples were included. Ten samples were used for total sEV isolation and analysis, and ten samples were used for tissue-specific sEV isolations (placental and fetal brain sEVs). No sample pooling was performed; each cord-blood sample was processed and analyzed individually to preserve inter-individual variability. Umbilical cord-blood was collected directly after delivery in K2EDTA tubes and processed according to ENVIRONAGE biobank procedures: within 20 min of collection, tubes were centrifuged at 3,200 rpm for 15 min to separate plasma, which was aliquoted (Eppendorf tubes) and stored at −80 °C until analysis. The archived samples used here were collected between 24 January 2014 and 23 November 2020, corresponding to a cryostorage duration at the time of sEV isolation of 5.1–11.9 years (median 8.7 years; IQR 7.2–9.9 years). All sEV isolations were performed from single-thaw plasma aliquots (one freeze–thaw cycle only; no repeated thawing/refreezing).

Using the merged address-based and placental datasets, we classified the biobank samples into three BC-exposure strata defined by the average BC particle concentration measured in each group's placentas: low (mean ≈ 2.6 × 103 particles mm^{-3}), moderate (≈ 2.3 × 104 particles mm^{-3}), and high (≈ 9.8 × 104 particles mm^{-3}). This grouping ensures that our sEV analyses span wide prenatal BC-exposure gradient represented in the cohort.

2.3. Isolation and characterization of sEVs

2.3.1. Control of environmental contamination during sEV extraction

As BC is a trace-level signal, we implemented measures to minimize and monitor exogenous particle contamination during processing. All open-tube steps were performed in a laminar-flow/biosafety cabinet providing HEPA-filtered unidirectional airflow. Isolation was conducted in a dedicated clean area (no combustion sources; no open windows), samples were kept capped whenever possible, and handling was performed with powder-free nitrile gloves and lab coats while minimizing movement/speaking over open tubes. Work surfaces and pipettes were wiped with 70 % ethanol prior to processing. PBS and wash buffers were 0.22 μm filtered before use to reduce particulate background. In each batch, magnetic-bead-only procedural controls were carried through the complete workflow and assessed in parallel to monitor potential background/contamination. Reporting follows established EV guidelines emphasizing documentation of pre-analytical variables and controls (Welsh et al., 2024).

Total sEVs were isolated from 250 μL of cord-blood plasma using an Exo-spin™ Mini size-exclusion chromatography kit (Cell Guidance Systems, EX02) according to the manufacturer's protocol. Briefly, plasma was first centrifuged at 300 × g for 10 min at 4 °C to remove any cells, then at 16,000 × g for 20 min at 4 °C to pellet cell debris. sEVs were precipitated with the Exo-spin reagent and further purified by size-exclusion chromatography. The purified sEV fraction was concentrated and resuspended in phosphate-buffered saline (PBS) and stored at −80 °C until analysis. For controlling of environmental/particle contamination, all centrifugation and incubation steps were performed in tightly closed polypropylene tubes. Open-tube handling (pipetting, resuspension, wash steps) was limited to brief steps performed under a

laminar-flow/biosafety cabinet. PBS and wash buffers were 0.22 μm filtered prior to use. These measures were implemented to minimize exogenous particulate deposition during sEV isolation.

Placental and fetal-brain sEVs were isolated from the total sEV preparation by immunoaffinity capture. Pre-purified sEVs were incubated with magnetic beads (Thermo Fisher Scientific, Cat. No. 11206D) conjugated to biotinylated antibodies targeting PLAP (placental alkaline phosphatase; Thermo Fisher Scientific, Cat. 15537396) to capture placental sEVs, or biotinylated antibodies targeting Contactin-2 (R&D Systems, Cat. MAB17141) to capture fetal-brain sEVs. Antibodies against Contactin-2 were biotinylated in-house using EZ-Link™ Sulfo-NHS-Biotin (Thermo Fisher, Cat. 21326), and excess biotin was removed with Zeba™ desalting columns (Thermo Fisher, Cat. 89882). SEVs were incubated with the antibody-conjugated beads for 2 h at room temperature under gentle rotation. Magnetic separation was then used to retrieve the bead-bound sEVs, which were washed in PBS and stored at −80 °C until further analysis.

Isolated sEVs were characterized for size and identity (Welsh et al., 2024). NTA was performed using a ZetaView® instrument (Particle Metrix) to determine vesicle size distribution and concentration. Cryo-TEM imaging on a Thermo Fisher Tecnai Arctica microscope confirmed vesicle morphology and integrity. Conventional TEM was used to visualize sEVs attached to magnetic beads. For TEM, magnetic bead-coupled sEVs were fixed in 4 % paraformaldehyde, embedded in 12 % gelatin, infused with 2.3 M sucrose, and frozen in liquid nitrogen. Ultrathin cryosections were prepared using a Leica EM Ultracut UC6/FC6 cryo-ultramicrotome, collected in 2 % methylcellulose (2.3 M sucrose), and embedded in 1.8 % methylcellulose with 0.4 % uranyl acetate. Imaging was performed on a Tecnai Spirit Electron Microscope (Thermo Fisher Scientific) with an Eagle 4kx4k CCD camera. (Bentaleb et al., 2022) Western blotting was carried out to detect canonical sEV protein markers (CD9, CD63, CD81) (Kowal et al., 2017) and to confirm the presence of tissue-specific markers in the immunocaptured subfractions (PLAP for placental sEVs; Contactin-2, and L1CAM for fetal-brain sEVs).

2.3.2. Fluorescent labeling of sEVs

sEV membranes were fluorescently labeled with BODIPY® TR ceramide (Thermo Fisher, Cat. B34400). In brief, 100 μL of sEV suspension was incubated with 1 μL of 1 mM BODIPY TR ceramide at 37 °C for 20 min. After labeling, excess dye was removed. Labeled total sEVs were purified again using the Exo-spin column, and bead-bound sEV samples were washed three times with PBS using magnetic separation to remove unbound dye.

2.3.3. Label-free two-photon imaging and quantification of black carbon associated with sEVs

BC was visualized with a label-free white-light multiphoton technique that our group has previously validated for placental tissue and blood samples. (Vanbrabant et al., 2024; Bové et al., 2019; Bongaerts et al., 2022; Bové et al., 2016) This method exploits the nonlinear optical properties of carbonaceous particles, characterized by broadband visible emission and an instantaneous temporal response upon excitation (Bové et al., 2016).

sEV samples, either in suspension or immunocaptured on antibody-coated magnetic beads, were mounted in shallow wells on glass slides and imaged using a Zeiss LSM 880 confocal/multiphoton microscope. Imaging chambers were prepared using cleaned slides/coverslips and sealed immediately after sample loading to prevent contact with ambient air during imaging, following the CarbonSense SOP (Cleaning and Creating Imaging Chambers for BC detection in biofluids; Supplementary File 1). The system was equipped with a mode-locked Ti:sapphire femtosecond laser (Mai Tai DeepSee, Spectra-Physics; 810 nm excitation, ~150 fs pulse width, 80 MHz repetition rate). High-resolution imaging was performed using a Plan-Apochromat 63×/1.4NA oil-immersion objective. Emission signals were collected in non-descanned detection mode through two spectral windows: 400–410 nm for second-harmonic generation (SHG, displayed in red) and 450–650 nm for two-photon autofluorescence (TPAF, displayed in green). Although these spectral windows are commonly used to visualize endogenous tissue signals (SHG at 400–410 nm and TPAF at 450–650 nm), BC identification in this study relies on the previously validated femtosecond-excited, non-incandescence broadband "white-light" emission of carbonaceous particles, which is detected across the visible spectrum and therefore appears in both windows. (Vanbrabant et al., 2024; Bové et al., 2019; Bové et al., 2016) Accordingly, SHG/TPAF channels provide structural/context information, while BC is operationally defined by its broadband emission recorded in both bands (dual-window criterion). (Bové et al., 2019; Bové et al., 2016) A voxel was classified as BC only when it exceeded fixed thresholds in both bands (50 AU and 100 AU, corresponding to 19.6 % and 39.2 % of the detector range, respectively); the logical AND of these masks defined the BC signal. Membrane fluorescence from BODIPY-TR-labelled vesicles was recorded in descanned mode at 580–620 nm.

Z-stack imaging (10 optical sections across a 1 μm total depth) was conducted to assess three-dimensional localization of BC within bead-bound sEVs. Due to the axial resolution limit (~350 nm), individual sEVs (~100 nm) could not be fully resolved; however, BC-positive vesicles typically appeared in $\leq$ 4 consecutive optical sections. Orthogonal XZ and YZ reconstructions were consistent with vesicle-associated BC within the limits of confocal axial resolution for nano-sized sEVs. However, because individual sEVs (~100 nm) are below the diffraction limit and the confocal axial resolution, these data cannot definitively distinguish intraluminal BC from BC adsorbed to the outer vesicle surface; unambiguous bilayer-level localization would require higher-resolution 3D EM approaches (e.g., cryo-electron tomography).

Image processing and analysis were conducted using Fiji/ImageJ v1.55. SHG and TPAF channels were thresholded individually using manual thresholding on a per-stack basis, isolating high-intensity pixels (top ~ 40 % for SHG and ~ 20 % for TPAF), consistent with the known saturation characteristics of BC. (Bové et al., 2019) Thresholded images were merged, and co-localized signals appeared white, representing BC particles. Co-localization between the sEV membrane signal (cyan, BODIPY TR) and the BC signal (white) was assessed using the JaCoP (Just Another Colocalization Plugin) in Fiji.

Enumeration of individual sEVs was performed using the EVAnalyzer plugin with MaxEntropy thresholding, enabling segmentation and quantification of vesicle counts and their overlap with BC signals. All analyses were performed blinded to sample identity, and thresholding parameters were applied consistently across all samples.

Given the diffraction-limited lateral resolution (300–400 nm), each BC signal likely corresponds to a single nanoparticle or a small agglomerate. Thus, BC quantification is relative rather than absolute, in agreement with previous findings in placental tissue imaging. (Bové et al., 2019; Bongaerts et al., 2022).

2.3.4. Image processing and quantitative extraction

All image-based measurements were performed in Fiji/ImageJ v1.55 (NIH) (Schneider et al., 2012). Co-localization between the sEV-membrane signal (BODIPY TR) and the BC signal was quantified with the JaCoP – Just Another Colocalization Plugin (Bolte and Cordelières, 2006), which reports Manders' overlap coefficients (M_1 and M_2) and Pearson's correlation coefficient (r). These JaCoP outputs are within-image (pixel-intensity) colocalization metrics; we did not perform between-participant correlation analyses (e.g., Pearson/Spearman) between EV/BC variables. Thresholds were applied uniformly within each experimental group: for unfractionated cord-plasma images the thresholds were set to 2 AU for BC and 20 AU for sEVs; for both placental ($PLAP^+$) and fetal-brain ($Contactin\text{-}2^+$) images the thresholds were 2 AU for BC and 36 AU for magnetic beads. Enumeration of individual sEVs was carried out with the EVAnalyzer plugin using MaxEntropy thresholding. The details for each image stack and sEV counting are listed in

Supplementary Table 1.

2.4. Statistical analysis

Data exported from ImageJ were processed in GraphPad Prism 10 (GraphPad Software, San Diego, CA). For each vesicle population we report the arithmetic mean, range and two-sided 95 % confidence interval (CI). JaCoP-derived Pearson's r and Manders' coefficients are pixel-intensity colocalization metrics within each image and should not be interpreted as between-participant correlations. To explore between-participant associations with exposure proxies, we used Spearman correlation between maternal exposure estimates (residential BC; placental BC) and per-sample sEV-associated BC metrics (mean across technical repeats).

3. Results

3.1. Characterization of small extracellular vesicles

We successfully isolated total sEVs from cord-blood plasma and characterized them using nanoparticle tracking analysis (NTA), cryogenic transmission electron microscopy (cryo-TEM), and Western blotting. NTA revealed a size distribution with a predominant peak at ~ 100 nm for the isolated vesicles (Fig. 1A), consistent with expected sEV profiles. (Welsh et al., 2024) The particle concentrations indicated effective recovery of sEVs from cord-blood plasma. Cryo-TEM imaging demonstrated that the sEVs were roughly spherical with intact lipid bilayers (Fig. 1B and supplementary file 2), confirming the high structural integrity and quality of the isolates. Western blotting confirmed the presence of established sEV surface protein markers CD9 (24 kDa), CD63 (30–60 kDa), and CD81 (26 kDa) in our samples (Fig. 1C and supplementary file 3), supporting the identification of these vesicles as bona fide sEVs.

3.2. Isolation of sEVs and tissue-specific sEVs

To investigate tissue-specific sEV subsets, we enriched placental and fetal-brain sEVs from the total cord-blood sEV pool via immunocapture. Magnetic beads conjugated with antibodies against PLAP were used to isolate placental sEVs, and beads with antibodies against Contactin-2 were used to capture fetal-brain sEVs. TEM imaging confirmed robust binding of sEVs to the antibody-coated beads (Fig. 1D1- D3), whereas control beads lacking these antibodies did not capture any vesicles. Because the immunocapture platform consists of micron-sized beads, Fig. D1-2 visualizes beads with attached nanoscale sEVs (red arrows) rather than vesicle size; vesicle size is supported by NTA (Fig. 1A) and cryo-TEM (Fig. 1B). Western blot analysis further validated the specificity of the isolation: PLAP was detected exclusively in placental sEV isolates, and neural markers, including Contactin-2 and L1CAM, were detected in fetal-brain sEV isolates (Fig. 1E). These results confirm the successful enrichment of placental and neural-specific sEV populations from cord-blood.

3.3. Quantification of BC co-localization

3.3.1. Nonspecific BC binding to magnetic beads

To exclude the possibility of nonspecific BC binding to the capture beads, we performed control experiments using magnetic beads incubated under identical conditions but without coupled antibodies. Quantitative imaging of these control beads (n = 21) revealed a very low average of BC particles per bead (0.7 ± 1.7 particles/bead), with the majority of samples (17 out of 21) showing no BC signal. In contrast,

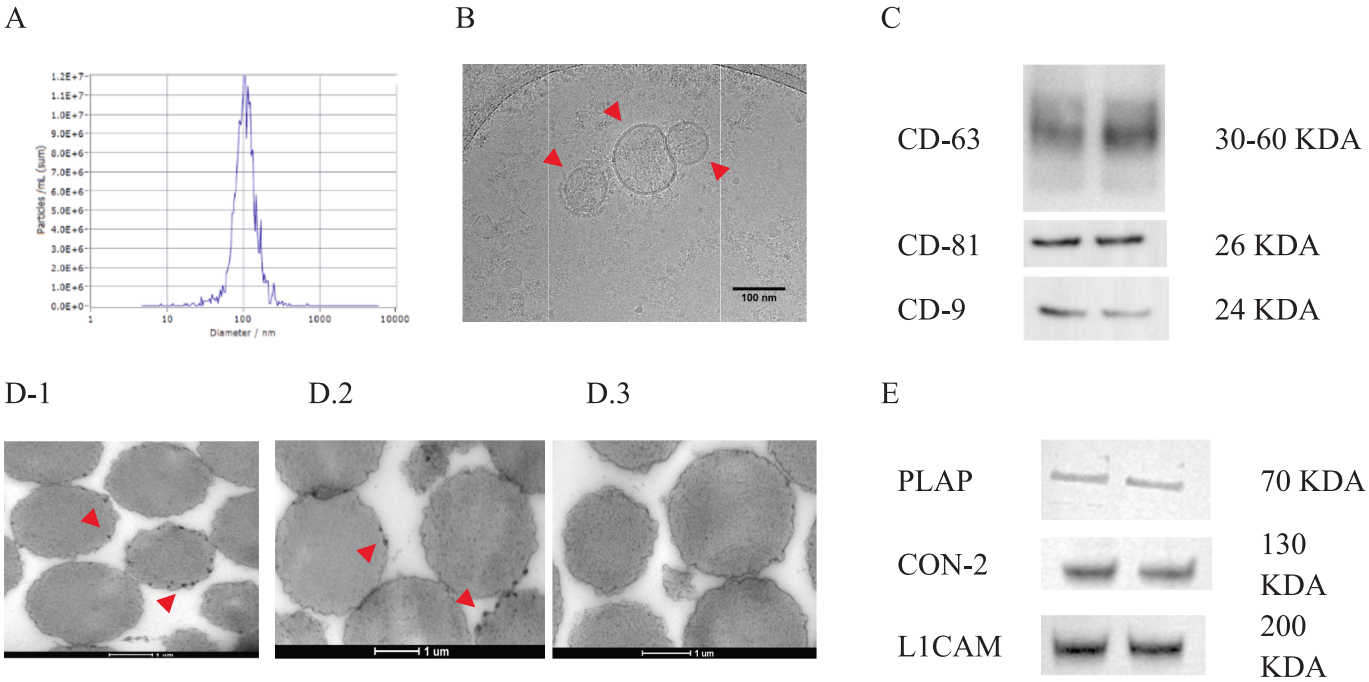

Fig. 1. Characterization of small extracellular vesicles (sEVs) from cord-blood. (A) Nanoparticle tracking analysis of cord-blood plasma total sEVs shows a size distribution with a predominant peak at ~ 100 nm, consistent with expected vesicle size. (B) Cryo-TEM image of isolated total sEVs, demonstrating their spherical morphology and intact lipid bilayer (scale bar: 100 nm). Red arrows indicate sEVs (C) Western blot detection of canonical total sEV protein markers (CD9, CD63, CD81) in the isolated vesicles, confirming their identity as sEVs. (D1–D3) Negative-stain TEM of micron-sized magnetic microbeads (~1 μm) used for immunocapture of tissue-enriched sEVs (scale bars: 1 μm). The large structures are beads; nanoscale sEVs are the particles attached to the bead surface (red arrows) and bead size does not reflect vesicle diameter. (D1) Placental sEVs captured by PLAP-conjugated beads. (D2) Fetal brain sEVs captured by Contactin-2-conjugated beads. (D3) Control beads with no antibody (showing no vesicle binding). (E) Western blot analysis of tissue-specific markers in the sEV subpopulations: PLAP (placental sEV marker) is present only in placental sEV isolates, whereas Contactin-2 (CNTN2) and L1CAM (neural markers) are present in fetal brain sEV isolates. (For interpretation of the references to colour in this figure legend, the reader is referred to the web version of this article.)

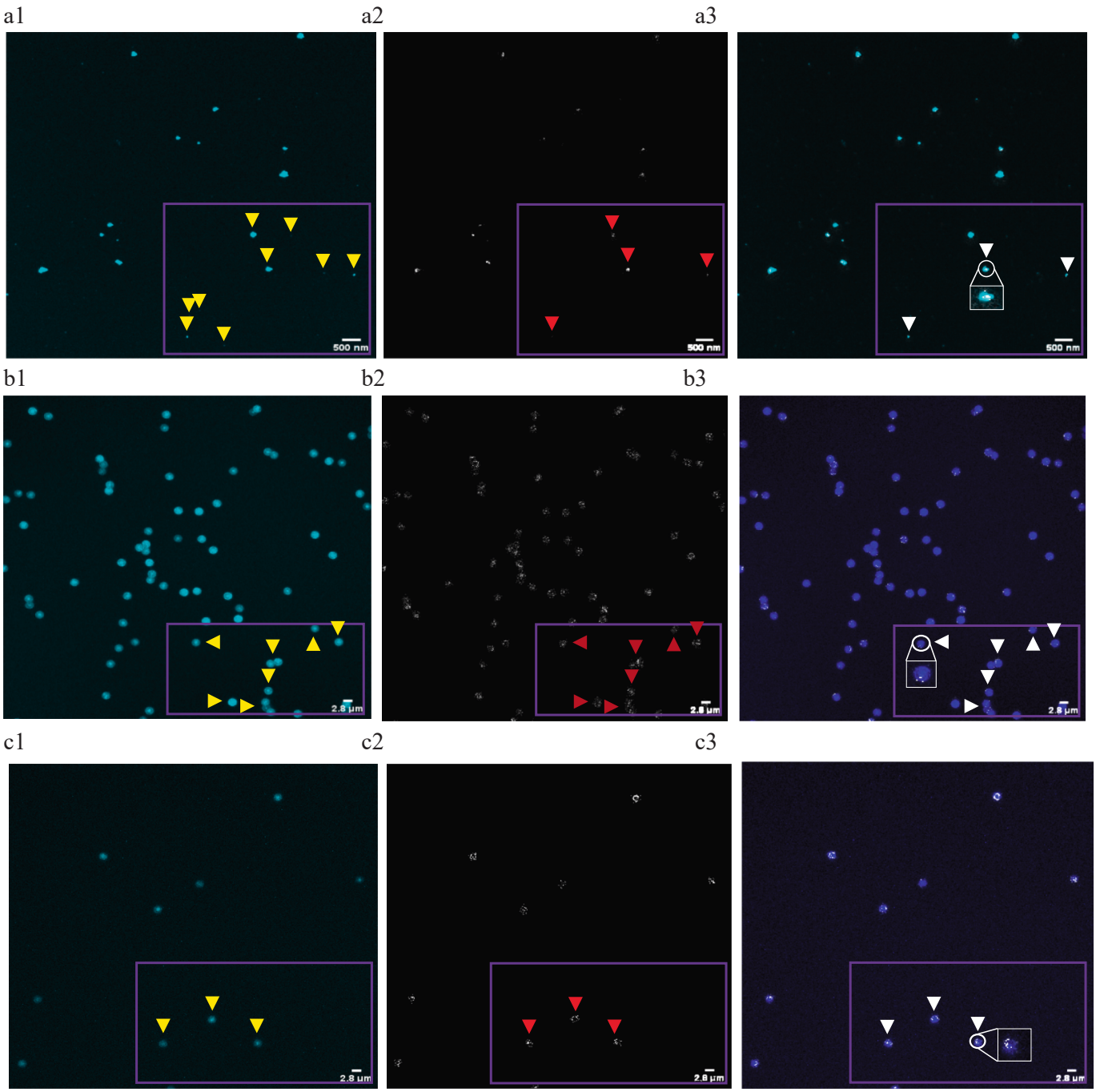

Fig. 2. Label-free two-photon imaging reveals black carbon (BC) co-localization within cord-blood-derived small extracellular vesicles (sEVs). Representative two-photon images of total cord-blood sEVs (top row, a1–a3), placenta-derived PLAP^{+} sEVs captured on beads (middle row, b1–b3), and fetal brain-derived Contactin-2^{+} sEVs captured on magnetic beads (bottom row, c1–c3). Panel A1 shows free sEVs with membranes labeled using BODIPY TR ceramide (cyan), while panels b1 and c1 depict bead-bound sEVs with visible membrane labeling. Panels a2, b2, and c2 display black carbon (BC) particles identified through co-localization of second harmonic generation (SHG, red) and two-photon autofluorescence (TPAF, green) signals, resulting in a white emission under femtosecond-pulsed laser excitation. Panel a3 shows a merged image confirming spatial co-localization of BC (white) within free sEVs (cyan), while panels b3 and c3 show BC co-localized with sEVs bound to beads(blue). Yellow arrows indicate sEVs or sEV-bead complexes, red arrows highlight BC signals, and white arrows denote regions of co-localized BC and sEVs. Arrows are selectively displayed within the purple boxes to highlight key features while minimizing visual clutter in the overall image. The white boxes indicate regions of interest that are magnified to show detailed colocalization. (For interpretation of the references to colour in this figure legend, the reader is referred to the web version of this article.)

beads coupled with antibodies and incubated with sEV-containing samples exhibited significantly higher BC counts, reaching up to 68 particles/bead for placental sEV samples and up to 84 particles/bead for fetal-brain sEV samples. Furthermore, while BC signals were detected randomly attached to the surface of the control beads, no sEV signals were observed. These observations confirm that the BC signals observed in the sEV-bound samples represent BC associated with the vesicles rather than nonspecific attachment to the beads.

3.3.2. *Total sEVs in cord-blood*

A total of 1,406 total cord-plasma sEVs were analyzed, revealing 313 individual BC particles. On a per-image basis a mean of 27 % of vesicles

carried at least one BC particle (range 0–100 %) (Fig. 2A).

Manders' M1 (BC → sEV; fraction of BC fluorescence that overlaps vesicle signal) averaged 0.44 (0.26–0.75), indicating that roughly 44 % of the total BC signal was confined to vesicles. By contrast, Manders' M2 (sEV → BC; fraction of vesicle fluorescence that overlaps BC) averaged 0.23 (0.04–0.52), showing that only about one quarter of the vesicle signal co-localised with BC, consistent with the majority of vesicles being BC-negative. Pixel-wise Pearson's r (JACoP) between the BC and sEV membrane channels was low (mean r ≈ 0.35, 0.01–0.62), further supporting limited co-localisation in this total sEV pool.

3.3.3. Placenta-derived (PLAP) sEVs

Placental sEVs isolated using PLAP-coated magnetic beads (n = 1,053 sEVs analyzed) also carried substantial amounts of BC, with 668 BC particles detected. The global BC: sEV ratio was 0.63, and on average 54 % of PLAP$^+$ vesicles were BC-positive (range 0–100 %)(Fig. 2b). Manders' M1 (BC → sEV; fraction of BC fluorescence on vesicles) averaged 0.35 (0.05–0.62), and M2 (sEV → BC; fraction of vesicle fluorescence that overlaps BC) averaged 0.87 (0.53–0.99), indicating that while roughly one-third of the total BC signal was vesicle-bound, most placental vesicles themselves contained BC. Pixel-wise Pearson's r (JaCoP) was moderately high (mean r = 0.77, 0.55–0.87). Notably, three preparations from one of the samples displayed ≤ 2 BC particles despite abundant PLAP signal, underlining inter-individual variability. These data suggest that placenta-derived sEVs can effectively sequester and transport BC, though the extent varies greatly among individuals (potentially due to differences in maternal exposure levels or placental filtering efficiency).

3.3.4. Fetal brain-derived sEVs

In fetal-brain sEVs isolated with Contactin-2 beads (n = 1,399 vesicles), we detected 1,053 BC particles. On average, 68 % of brain-derived vesicles contained at least one BC particle (range 11–100 %) (Fig. 2c). Manders' M1 (BC → sEV; fraction of BC fluorescence on vesicles) averaged 0.45 (0.12–0.78), showing that roughly half of the total BC signal was confined to vesicles. Manders' M2 (sEV → BC; fraction of vesicle fluorescence that overlaps BC) was much higher, averaging 0.91 (0.82–1.00); thus ≈ 90 % of the vesicle signal co-localized with BC, consistent with the high proportion of BC-positive vesicles. Pixel-wise Pearson's r (JaCoP) correlation was likewise strong (mean r ≈ 0.84, 0.75–0.98). Together, these data indicate that fetal-brain (Contactin-2$^+$) sEV fractions show the highest BC association among the analyzed vesicle populations in fetal circulation, consistent with preferential BC association/enrichment in this vesicle-enriched fraction.

Quantitative imaging revealed that BC is highly enriched in specialised fetal sEV fractions. Fetal-brain (CNTN2$^+$) vesicles were the most heavily laden: on average 68 % of vesicles carried at least one BC particle (range 11–100 %). Manders M1, which measures the fraction of total BC fluorescence that co-localizes with vesicles, averaged 0.45, whereas M2, the fraction of total vesicle fluorescence that overlaps BC, averaged 0.91, indicating that more than 90 % of the sEV signal in this fraction was associated with BC. Placental PLAP$^+$ vesicles showed an intermediate enrichment, with roughly 54 % BC-positive vesicles and an average M2 of 0.87. By contrast, the unfractionated cord-plasma pool contained BC in only about 27 % of vesicles and exhibited a much lower M2 of 0.23. Manders coefficients were calculated across the full fluorescence signal in each field, so vesicles lacking BC are included in the reported means; thus the high M2 value for fetal-brain sEVs still reflects the entire vesicle population. Collectively, these data indicate that vesicles of fetal origin, particularly those released from the developing brain and placenta, show higher BC association in our measurements. The strong BC signal observed in PLAP$^+$ trophoblastic vesicle fractions is consistent with placental-origin sEVs being a potential contributor to BC association in the fetal compartment. However, our data do not establish that vesicular trafficking is the primary mechanism of BC transfer, and other carriers/pathways also contribute. Exploratory Spearman correlations between exposure proxies (modeled residential BC and placental BC, particles/mm^3) and sEV-associated BC metrics did not show statistically robust monotonic associations in this pilot (all p ≥ 0.13; Supplementary Table 2).

4. Discussion

Air-pollution exposure, particularly to combustion-derived fine particles such as BC, has been linked to respiratory, cardiovascular and neurodevelopmental morbidity. (Manisalidis et al., 2020) Here we show that BC is detectable in association with cord-blood sEV preparations and in immuno-enriched vesicle fractions of placental or fetal-brain origin. These observations support the presence of sEV-associated BC in fetal circulation, while not establishing that sEVs are the primary or exclusive transport mechanism. By visualising BC within cord-blood total sEVs and in vesicle fractions of placental or fetal-brain origin, our findings are consistent with sEVs being a plausible biological carrier contributing to BC transport in fetal circulation. Given the current imaging resolution, our data support sEV-associated BC (surface-associated and/or intravesicular) rather than definitive intraluminal encapsulation. Our findings extend earlier reports of BC on the fetal side of the placenta and in fetal circulation (Bové et al., 2019; Bongaerts et al., 2022) by identifying vesicle-enriched fractions in which BC association can be quantified. Recognising sEVs as pollutant carriers underscores the complexity of nanoparticle dissemination in pregnancy and highlights the need for strategies to minimize maternal BC exposure.

sEVs are established mediators of intercellular communication, transporting nucleic acids, proteins and lipids across biological barriers. (Di Bella, 2022) We now demonstrate that BC can be detected in association with sEV-enriched preparations in fetal cord-blood. Among cord-blood vesicles, BC loading was highly tissue-specific: fetal-brain-derived sEVs carried the greatest burden, placental PLAP$^+$ vesicles were intermediate and the unfractionated plasma pool contained the least BC.

The reported BC-positivity values (e.g., PLAP$^+$ vs CNTN2$^+$) represent the fraction of vesicles carrying ≥ 1 BC particle within two immuno-enriched EV fractions, and should not be interpreted as a direct measure of relative BC burden in placenta versus fetal brain. Marker-based immuno-capture yields enriched rather than pure EV populations, and positivity rates can be influenced by EV heterogeneity and capture efficiency. (Welsh et al., 2024; Van Deun et al., 2017) Importantly, the placenta is not an obligatory "sink" for black carbon before fetal exposure occurs: ambient BC has been detected on the fetal side of human placenta, consistent with transplacental transport, (Bové et al., 2019) and carbonaceous air pollution particles have been reported to cross the placenta and translocate into fetal circulation and fetal organs during gestation. (Bongaerts et al., 2022; Bongaerts et al., 2020) Mechanistically, particle transfer across the placental barrier is described as particle-property-dependent and may involve transcellular uptake/transcytosis and/or paracellular passage rather than requiring proportional placental accumulation. (Bongaerts et al., 2020) In addition, placental EV release changes across gestation and placental EVs are abundant near term, which can increase the denominator (total PLAP$^+$ vesicles) and reduce the BC-positive fraction even in the presence of placental BC. (Salomon et al., 2014; Mitchell et al., 2015) Conversely, EVs contribute to CNS development and intercellular signaling, and EV secretion is also discussed as a route for exporting unwanted material and maintaining cellular homeostasis; therefore, higher BC-positivity within a brain-enriched EV fraction at delivery is biologically plausible once BC has entered the fetal compartment. (Bahram Sangani et al., 2021; Vidal, 2019) Finally, differential physicochemical association of carbonaceous particles with lipid interfaces and corona effects may vary between EV subtypes and could contribute to different positivity fractions in PLAP$^+$ versus CNTN2$^+$ fractions. (Pajnič et al., 2015; Pan et al., 2022).

Because the fetal brain undergoes rapid neurogenesis, synaptogenesis and myelination, it is especially vulnerable to oxidative stress

and inflammation elicited by particulate matter. Epidemiological studies have linked prenatal particle exposure to increased risks of autism spectrum disorder, attention-deficit/hyperactivity disorder (Zhang et al., 2024; Perera et al., 2024), and later cognitive deficits (Campbell, 2023), and we have recently shown that BC accumulates in memory-related brain regions. (Vanbrabant et al., 2024) Given that sEVs readily cross the blood–brain barrier, (Banks et al., 2020), the detection of BC in a fetal-brain-enriched vesicle fraction at delivery is biologically plausible and may be relevant to developing neural circuits if such vesicle-associated material reaches sensitive tissues (Shang et al., 2024).

The molecular determinants of BC incorporation into sEVs remain to be elucidated. Particles could be passively engulfed during vesicle biogenesis, or actively packaged through specific protein- or lipid-mediated interactions; other extracellular carriers (larger vesicles, lipoproteins or phagocytes) may also contribute. Future work should quantify the relative importance of these parallel routes and define the proteomic and lipidomic signatures that promote BC loading, as these may offer therapeutic entry points. The high inter-individual variability we observed mirrors differences in maternal exposure and placental handling and suggests that measuring BC in circulating sEVs, particularly those of placental or fetal origin, could serve as a minimally invasive biomarker of fetal pollutant burden. Large-scale studies correlating sEV-associated BC with external exposure metrics and infant outcomes will be required to validate this possibility.

Finally, our data invite exploration of whether the vesicle pathway extends to other ultrafine particles or toxicants. If so, sEVs may represent a common conduit through which diverse environmental nanoparticles breach the placental barrier. Mapping this broader pollutant "cargoome" will clarify the full spectrum of fetal exposures and inform efforts to protect the developing child.

In summary, we provide the first evidence that BC is detectable in association with circulating sEVs in human fetal cord-blood, consistent with vesicle-associated carriage following transplacental particle transfer. While vesicular sequestration may shield the fetus from some free-particle toxicity, it simultaneously delivers pollutants deep into sensitive tissues, including the brain. These insights refine our understanding of placental permeability, reveal a promising source of exposure biomarkers and point towards new intervention targets for safeguarding early human development in an increasingly polluted world.

4.1. Limitations

Limitations and exposure–response inference: This proof-of-concept study has a limited biological sample size (20 participants overall; n = 10 per EV fraction for the primary analyses), which constrains statistical power and generalizability. Although multiple technical repeats were acquired per participant to improve precision, these do not increase biological power. In exploratory Spearman analyses using modeled residential BC and placental BC (particles/mm^3), we did not observe statistically robust monotonic correlations with sEV-associated BC metrics (all $p \geq 0.13$). Larger, powered studies are required to quantify exposure–response relationships with modeled $PM_{2.5}$/BC across pregnancy windows and to link sEV-associated BC to infant outcomes.

CRediT authorship contribution statement

Houman Kahroba: Writing – original draft, Formal analysis, Data curation, Conceptualization. **Kenneth Vanbrabant:** Writing – review & editing, Formal analysis, Data curation. **Julian Krauskopf:** Writing – review & editing, Validation, Supervision. **Jacco Briedé:** Writing – review & editing, Validation, Supervision. **Marcel Ameloot:** Writing – review & editing, Validation. **Michelle Plusquin:** Writing – review & editing, Validation. **Maarten Roeffaers:** Writing – review & editing, Validation. **Theo M. de Kok:** Writing – review & editing, Validation, Supervision. **Tim Nawrot:** Writing – review & editing, Validation, Supervision.

Funding

ENVIRONAGE is supported by the Methusalem programme, the Maastricht University-Hasselt University Special Research Fund (BOF) grant (to H.K.), and the European Union's Horizon Europe programme through the MISTRAL project (Grant Agreement No. 101095119).

Declaration of competing interest

The authors declare that they have no known competing financial interests or personal relationships that could have appeared to influence the work reported in this paper.

Acknowledgements

We are grateful to the participating mothers and the clinical staff of East-Limburg Hospital for their support during sample collection. This work was supported by the ENVIRONAGE birth cohort project at Hasselt University, Belgium and by the Department of Translational Genomics at Maastricht University, The Netherlands. The authors also thank the technical staff at Maastricht University for their contributions to the experimental procedures.

Appendix A. Supplementary data

Supplementary data to this article can be found online at https://doi.org/10.1016/j.envint.2026.110186.

Data availability

Data will be made available on request.

References

Bahram Sangani, N., Gomes, A.R., Curfs, L.M.G., Reutelingsperger, C.P., 2021. The role of extracellular vesicles during CNS development. Prog. Neurobiol. 205. https://doi.org/10.1016/j.pneurobio.2021.102124.

Banks WA, Sharma P, Bullock KM, Hansen KM, Ludwig N, Whiteside TL. Transport of Extracellular Vesicles across the Blood-Brain Barrier: Brain Pharmacokinetics and Effects of Inflammation. *Int J Mol Sci 2020, Vol 21, Page 4407*. 2020;21(12):4407. doi:10.3390/IJMS21124407.

Benabed, A., Boulbair, A., 2022. PM10, PM2.5, PM1, and PM0.1 resuspension due to human walking. Air Qual Atmos Heal. 15 (9). https://doi.org/10.1007/S11869-022-01201-3.

Bentaleb, C., Hervouet, K., Montpellier, C., et al., 2022. The endocytic recycling compartment serves as a viral factory for hepatitis E virus. Cell. Mol. Life Sci. 79 (12), 615. https://doi.org/10.1007/S00018-022-04646-Y.

Binter, A.C., Kusters, M.S.W., van den Dries, M.A., et al., 2022. Air pollution, white matter microstructure, and brain volumes: periods of susceptibility from pregnancy to preadolescence. Environ. Pollut. 313. https://doi.org/10.1016/j.envpol.2022.120109.

Bolte, S., Cordelières, F.P., 2006. A guided tour into subcellular colocalization analysis in light microscopy. J. Microsc. 224 (3), 213–232. https://doi.org/10.1111/J.1365-2818.2006.01706.X.

Bongaerts, E., Nawrot, T.S., Van Pee, T., Ameloot, M., Bové, H., 2020. Translocation of (ultra)fine particles and nanoparticles across the placenta. Part. Fibre Toxicol. 17 (1), 56. https://doi.org/10.1186/s12989-020-00386-8.

Bongaerts, E., Lecante, L.L., Bové, H., et al., 2022. Maternal exposure to ambient black carbon particles and their presence in maternal and fetal circulation and organs: an analysis of two independent population-based observational studies. Lancet Planet Heal. 6 (10), e804–e811. https://doi.org/10.1016/S2542-5196(22)00200-5.

Bové, H., Steuwe, C., Fron, E., et al., 2016. Biocompatible label-free detection of carbon black particles by femtosecond pulsed laser microscopy. Nano Lett. 16 (5), 3173–3178. https://doi.org/10.1021/ACS.NANOLETT.6B00502.

Bové H, Bongaerts E, Slenders E, et al. Ambient black carbon particles reach the fetal side of human placenta. *Nat Commun 2019 101*. 2019;10(1):1-7. doi:10.1038/s41467-019-11654-3.

Buerki-Thurnherr, T., Von Mandach, U., Wick, P., 2012. Knocking at the door of the unborn child: engineered nanoparticles at the human placental barrier. Swiss Med. Wkly. 142 (APRIL). https://doi.org/10.4414/SMW.2012.13559.

Burkova, E.E., Sedykh, S.E., Nevinsky, G.A., 2021. Human placenta exosomes: biogenesis, isolation, composition, and prospects for use in diagnostics. Int. J. Mol. Sci. 22 (4), 2158. https://doi.org/10.3390/IJMS22042158.
Campbell, D.B., 2023. Air pollution exposure during pregnancy increases risk of neurodevelopmental disorders. Dev. Med. Child Neurol. 65 (6), 728–729. https://doi.org/10.1111/DMCN.15511.
Cheng, W., Zhang, W., Xia, X., et al., 2023. The domino effect in inhaled carbon black nanoparticles triggers bloodbrain barrier disruption via altering circulatory inflammation. Nano Today 48, 101721. https://doi.org/10.1016/J.NANTOD.2022.101721.
Deng, Y., Li, X., Li, X., et al., 2025. Association of early life exposure to PM2.5 and its components with offspring neurodevelopment: a prospective birth cohort study. Environ. Res. 266, 120552. https://doi.org/10.1016/J.ENVRES.2024.120552.
Di Bella, M.A., 2022. Overview and update on extracellular vesicles: considerations on exosomes and their application in modern medicine. Biology (Basel). 11 (6), 804. https://doi.org/10.3390/BIOLOGY11060804.
Goetzl, L., Stephens, A.J., Schlesinger, Y., et al., 2021. Fetal central nervous system derived extracellular vesicles: potential for non-invasive tracking of viral mediated fetal brain injury. Front. Virol. 1, 782863. https://doi.org/10.3389/FVIRO.2021.782863/BIBTEX.
Guxens, M., Aguilera, I., Ballester, F., et al., 2012. Prenatal exposure to residential air pollution and infant mental development: modulation by antioxidants and detoxification factors. Env Heal Perspect. 120 (1), 144–149. https://doi.org/10.1289/ehp.1103469.
Guxens, M., Garcia-Esteban, R., Giorgis-Allemand, L., et al., 2014. Air pollution during pregnancy and childhood cognitive and psychomotor development: six european birth cohorts. Epidemiology 25 (5), 636–647. https://doi.org/10.1097/EDE.0000000000000133.
Guxens, M., Lubczyńska, M.J., Muetzel, R.L., et al., 2018. Air pollution exposure during fetal life, brain morphology, and cognitive function in school-age children. Biol. Psychiatry 84 (4), 295–303. https://doi.org/10.1016/J.BIOPSYCH.2018.01.016.
Hurtado-Díaz, M., Riojas-Rodríguez, H., Rothenberg, S.J., et al., 2021. Prenatal PM2.5 exposure and neurodevelopment at 2 years of age in a birth cohort from Mexico city. Int. J. Hyg. Environ. Health 233. https://doi.org/10.1016/j.ijheh.2021.113695.
Janssen, B.G., Madhloum, N., Gyselaers, W., et al., 2017. Cohort profile: the ENVIRonmental influence on early AGEing (ENVIRONAGE): a birth cohort study. Int. J. Epidemiol. 46 (5), 1386–1387M. https://doi.org/10.1093/IJE/DYW269.
Kaisanlahti, A., Turunen, J., Byts, N., et al., 2023. Maternal microbiota communicates with the fetus through microbiota-derived extracellular vesicles. Microbiome 11 (1), 1–14. https://doi.org/10.1186/S40168-023-01694-9/FIGURES/6.
Kowal, E.J.K., Ter-Ovanesyan, D., Regev, A., Church, G.M., 2017. Extracellular vesicle isolation and analysis by western blotting. Methods Mol. Biol. 1660, 143–152. https://doi.org/10.1007/978-1-4939-7253-1_12.
Lei, X., Zhang, Y., Wang, Z., et al., 2022. Effects of prenatal exposure to PM2.5 and its composition on cognitive and motor functions in children at 12 months of age: the shanghai birth cohort study. Environ. Int. 170. https://doi.org/10.1016/j.envint.2022.107597.
Liu, N.M.N., Miyashita, L., Maher, B.A., et al., 2021. Evidence for the presence of air pollution nanoparticles in placental tissue cells. Sci. Total Environ. 751. https://doi.org/10.1016/j.scitotenv.2020.142235.
Liu, B., Fang, X., Strodl, E., et al., 2022. Fetal exposure to air pollution in late pregnancy significantly increases ADHD-risk behavior in early childhood. Int J Env Res Public Heal. 19 (17), 10482. https://doi.org/10.3390/ijerph191710482.
Loftus, C.T., Hazlehurst, M.F., Szpiro, A.A., et al., 2019. Prenatal air pollution and childhood IQ: preliminary evidence of effect modification by folate. Env Res. 176, 108505. https://doi.org/10.1016/j.envres.2019.05.036.
Manisalidis, I., Stavropoulou, E., Stavropoulos, A., Bezirtzoglou, E., 2020. Environmental and health impacts of air pollution. A Review. Front Public Heal. 8. https://doi.org/10.3389/FPUBH.2020.00014.
Martin-Bassols, N., De New, S.C., Shields, M.A., et al., 2023. Effect of in utero exposure to air pollution on adulthood hospitalizations. J. Urban Health 101 (1), 92. https://doi.org/10.1007/S11524-023-00803-1.
Mitchell, M.D., Peiris, H.N., Kobayashi, M., et al., 2015. Placental exosomes in normal and complicated pregnancy. Am. J. Obstet. Gynecol. 213 (4), S173–S181. https://doi.org/10.1016/J.AJOG.2015.07.001.
Nyadanu, S.D., Dunne, J., Tessema, G.A., et al., 2022. Prenatal exposure to ambient air pollution and adverse birth outcomes: an umbrella review of 36 systematic reviews and meta-analyses. Environ. Pollut. 306, 119465. https://doi.org/10.1016/J.ENVPOL.2022.119465.
Olusanya, B.O., Davis, A.C., Wertlieb, D., et al., 2018. Developmental disabilities among children younger than 5 years in 195 countries and territories, 1990–2016: a systematic analysis for the global burden of disease study 2016. Lancet Glob Heal. 6 (10), e1100–e1121. https://doi.org/10.1016/S2214-109X(18)30309-7.
Pajnič M, Drašler B, Šuštar V, et al. Effect of carbon black nanomaterial on biological membranes revealed by shape of human erythrocytes, platelets and phospholipid vesicles, *J Nanobiotechnology*. (2015)13(1) pp28 doi:10.1186/S12951-015-0087-3.
Pan, X., Qin, P., Liu, R., Yu, W., 2022. Molecular mechanism of coating carbon black nanoparticles with polycyclic aromatic hydrocarbons on the binding to serum albumin and the related cytotoxicity. J. Mol. Liq. 356, 119013. https://doi.org/10.1016/J.MOLLIQ.2022.119013.
Perera, F., Rauh, V., Whyatt, R., Tsai, W., Tang, D., Diaz, D., 2006. Effect of prenatal exposure to airborne polycyclic aromatic hydrocarbons on neurodevelopment in the first 3 years of life among inner-city children. Env Heal Perspect. 114 (114), 1287–1292.
Perera, F., Miao, Y., Ross, Z., et al., 2024. Prenatal exposure to air pollution during the early and middle stages of pregnancy is associated with adverse neurodevelopmental outcomes at ages 1 to 3 years. Environ. Health 23 (1), 95. https://doi.org/10.1186/S12940-024-01132-9/TABLES/4.
Peterson, B.S., Rauh, V.A., Bansal, R., et al., 2015. Effects of prenatal exposure to air pollutants (polycyclic aromatic hydrocarbons) on the development of brain white matter, cognition, and behavior in later childhood. JAMA Psychiat. 72 (6), 531–540. https://doi.org/10.1001/JAMAPSYCHIATRY.2015.57.
Peterson, B.S., Bansal, R., Sawardekar, S., et al., 2022. Prenatal exposure to air pollution is associated with altered brain structure, function, and metabolism in childhood. J Child Psychol. Psychiatry 63 (11), 1316–1331. https://doi.org/10.1111/JCPP.13578.
Pietroiusti, A., Vecchione, L., Malvindi, M.A., et al., 2018. Relevance to investigate different stages of pregnancy to highlight toxic effects of nanoparticles: the example of silica. Toxicol. Appl. Pharmacol. 342, 60–68. https://doi.org/10.1016/J.TAAP.2018.01.026.
Porta, D., 2016. Air pollution and cognitive development at age 7 in a prospective Italian Birth Cohort. Epidemiol Camb Mass. 27, 228–236.
Salomon, C., Torres, M.J., Kobayashi, M., et al., 2014. A gestational profile of placental exosomes in maternal plasma and their effects on endothelial cell migration. PLoS One 9 (6). https://doi.org/10.1371/JOURNAL.PONE.0098667.
Schneider, C.A., Rasband, W.S., Eliceiri, K.W., 2012. NIH image to ImageJ: 25 years of image analysis. Nat. Methods 9 (7), 671–675. https://doi.org/10.1038/NMETH.2089.
Shang, Y., Zhao, K., Xue, W., et al., 2024. Comparative assessment of acute neurotoxicity of real-world ultra-fine black carbon emitted from residential solid fuel combustion. Sci. Total Environ. 954, 176597. https://doi.org/10.1016/J.SCITOTENV.2024.176597.
Vanbrabant, K., Van Dam, D., Bongaerts, E., et al., 2024. Accumulation of ambient black carbon particles within key memory-related brain regions. JAMA Netw. Open 7 (4), E245678. https://doi.org/10.1001/JAMANETWORKOPEN.2024.5678.
Van Deun, J., Mestdagh, P., Agostinis, P., et al., 2017. EV-TRACK: transparent reporting and centralizing knowledge in extracellular vesicle research. Nat. Methods 14 (3), 228–232. https://doi.org/10.1038/NMETH.4185.
Vidal, M., 2019. Exosomes: revisiting their role as “garbage bags. Traffic 20 (11), 815–828. https://doi.org/10.1111/TRA.12687.
Welsh, J.A., Goberdhan, D.C.I., O’Driscoll, L., et al., 2024. Minimal information for studies of extracellular vesicles (MISEV2023): from basic to advanced approaches. J Extracell Vesicles. 13 (2). https://doi.org/10.1002/JEV2.12404.
Xu, X., Tao, S., Huang, L., et al., 2022. Maternal PM2.5 exposure during gestation and offspring neurodevelopment: findings from a prospective birth cohort study. Sci. Total Environ. 842. https://doi.org/10.1016/j.scitotenv.2022.156778.
Yi, C., Wang, Q., Qu, Y., Niu, J., Oliver, B.G., Chen, H., 2022. In-utero exposure to air pollution and early-life neural development and cognition. Ecotoxicol. Environ. Saf. 238. https://doi.org/10.1016/j.ecoenv.2022.113589.
Zhang, Y., Hu, Y., Talarico, R., et al., 2024. Prenatal exposure to ambient air pollution and cerebral palsy. JAMA Netw. Open 7 (7), e2420717–e. https://doi.org/10.1001/JAMANETWORKOPEN.2024.20717.